Applied and Computational Mechanics 20 (2026) XXX–YYY

# Kinematic and dynamic analysis of long-reach excavator equipped with drum cutter for dredging tasks

V.-H. Trinh[a], D.-V. Dang[a,*]

[a] *Institute of Vehicle and Energy Engineering, Le Quy Don Technical University, 100 000 Hanoi, Vietnam*

Received 21 April 2025; accepted 26 February 2026

**Abstract**

Operating characteristics (e.g., working area, kinematic and dynamic responses) of hydraulic excavators equipped with standard buckets is inherently defined by the dimensions of links, the corresponding characteristics of driving cylinders, and working conditions. For dredging construction, it is often necessary to integrate additional equipment into the original hydraulic excavator. Excavators mounted on pontoons and equipped with drum cutters are commonly employed for this purpose. Investigating the working performance of these devices is essential for integrating replacement equipment into excavators to meet specific design criteria, technical requirements, and operational spaces. The installation of an extended boom and the modification of the working attachment to meet dredging requirements have resulted in fundamental changes in the kinematic and dynamic characteristics of the working mechanism. Specifically, the addition of a long dynamic link and the presence of resistive forces that vary continuously due to the cutter teeth alternately entering and exiting the cutting zone represent key differences compared to the original machine. This study introduces an innovative configuration for a standard excavator by incorporating a long-reach arm and substituting the bucket with a drum cutter. This modification aims to enhance the excavator's effectiveness in dredging tasks. In addition to extending the reachable working area to more than twice that of the original configuration, the translational velocity of the drum cutter can exceed that of the actuating cylinder by over 30 times. From a dynamic response perspective, the cutting layer thickness is shown to have a pronounced influence on the variation of resistive force components, driving forces, and joint reaction forces, with the coefficient of variation (CV) reaching values of up to 38.02 %. When the cutting depth is increased by a factor of 1.5, the CV of the force components decreases by the same ratio; however, the magnitudes of these force components may increase by more than four times. Through a comprehensive kinematic and dynamic analysis, the modified working area and operating characteristics of the backhoe dredger are evaluated to ensure safe, efficient, and structurally optimized operations. The proposed design and the findings of the present research offer valuable insights and practical solutions for the manufacturing and improvement of dredging equipment.


*Keywords:* excavator, dredging, dynamic responses, drum cutter, kinematics, long-reach arm, working area

## 1. Introduction

Recently, opening maritime channels has become a complex and expensive task, essential for promoting the growth of maritime transportation and the economy. Selecting a mechanized solution for channel opening combines economic and technical considerations, requiring thorough evaluation of construction conditions, project specifics, timelines, and quality requirements [1, 26, 27]. Alongside deploying specialized equipment with high capacity and significant procurement costs, using excavators equipped with suction-cutting attachments mounted on floating pontoons is also a cost-effective and beneficial option [27, 32]. This has led to numerous studies focusing on the development of this equipment combination (i.e., amphibious excavator [20] and backhoe dredger [13, 14, 29]).

*Corresponding author. Tel.: +84 964 322 236, e-mail: dinh-vu.dang@lqdtu.edu.vn.
https://doi.org/10.24132/acm.2026.1002

The working area of excavators is a critical parameter [2, 28, 31, 34, 35] that defines the operational envelope within which the machine can perform in various tasks (i.e., excavation, demolition, heavy lifting, and dredging). The superior design of the original excavator work unit allows for flexible deployment and operation of auxiliary equipment to access various types of work targets. Furthermore, using a single base excavator while replacing or simultaneously improving the design of the boom and arm enables enhanced economic and technical efficiency as well as diverse construction organization options. When replacement equipment is mounted on the excavator, the operating range of the equipment assembly expands based on the original range, combined with the additional length of the attached components such as: long-reach excavators [18, 24], two or three arms [3, 35] and telescopic arm [15, 17]. In some cases, excavators need to be designed and modified to operate effectively in limited or specialized spaces [11, 21, 22, 36]. Cutter attached on excavators can be used for various tasks such as tunnel excavation [16], road repairing [7] and channel dredging [26]. Therefore, in addition to the aspects of extending the working range, increasing the excavator's functionality, and adding moving parts, controlling the equipment assembly becomes more complex. Ensuring safety for operators and surrounding equipment becomes a critical concern when studying integrated systems. Some extended studies, based on an established working region, can calculate and investigate the distribution of digging forces/torques that can be generated at any given point while also considering the uncertainties in the surveyed parameters [5, 38, 39]. This approach focuses on optimizing the machine configuration according to design requirements, ensuring adherence to technical standards and sufficient working space during construction operations [4, 9, 16].

The present paper aims to characterize the kinematic and dynamic analysis of a long-reach excavator equipped with a specialized drum cutter for dredging operations. The Denavit-Hartenberg (DH) transformation method is employed to systematically analyze the kinematics of the system. The study determines the modified working area of the equipment and compares it with that of the original excavator, revealing a significant expansion of the operational envelope. Therefore, the influence of the driving link velocities on the drum cutter's motion is examined, providing critical insights for optimizing the excavator's performance under various operational conditions. The kinematic analysis not only demonstrates the benefits of an extended working area but also contributes to improving the efficiency and precision of excavation tasks. In addition, dynamic analyses are conducted using the Adams software, a multibody system analysis package. These simulations capture both the coupled motions of the working assembly and the effects of actuator forces, providing a detailed understanding of the system behavior. Preliminary results clearly indicate the influence of cutting resistance forces and cutter leading methods on variations in hydraulic cylinder forces under representative dredging scenarios. The observed findings offer initial conclusions regarding the system dynamic characteristics and suggest directions for further research aimed at optimizing operational performance, enhancing structural stability, and improving energy efficiency. By integrating kinematic and dynamic analyses, this study establishes a comprehensive framework for the design, control, and operational optimization of long-reach dredging excavators, ultimately supporting safer, more efficient, and reliable dredging operations.

## 2. Formulations for working area of excavators with different equipment

In the operational assembly of an excavator, which consists of the boom, arm, and bucket, these components are interconnected through hinge joints $O_1$, $A_1$, $B_1$, see Fig. 1. The link dimensions $a_1 = O_1A_1$, $a_2 = A_1B_1$, $a_3 = B_1C_1$, along with the rotation angles around the

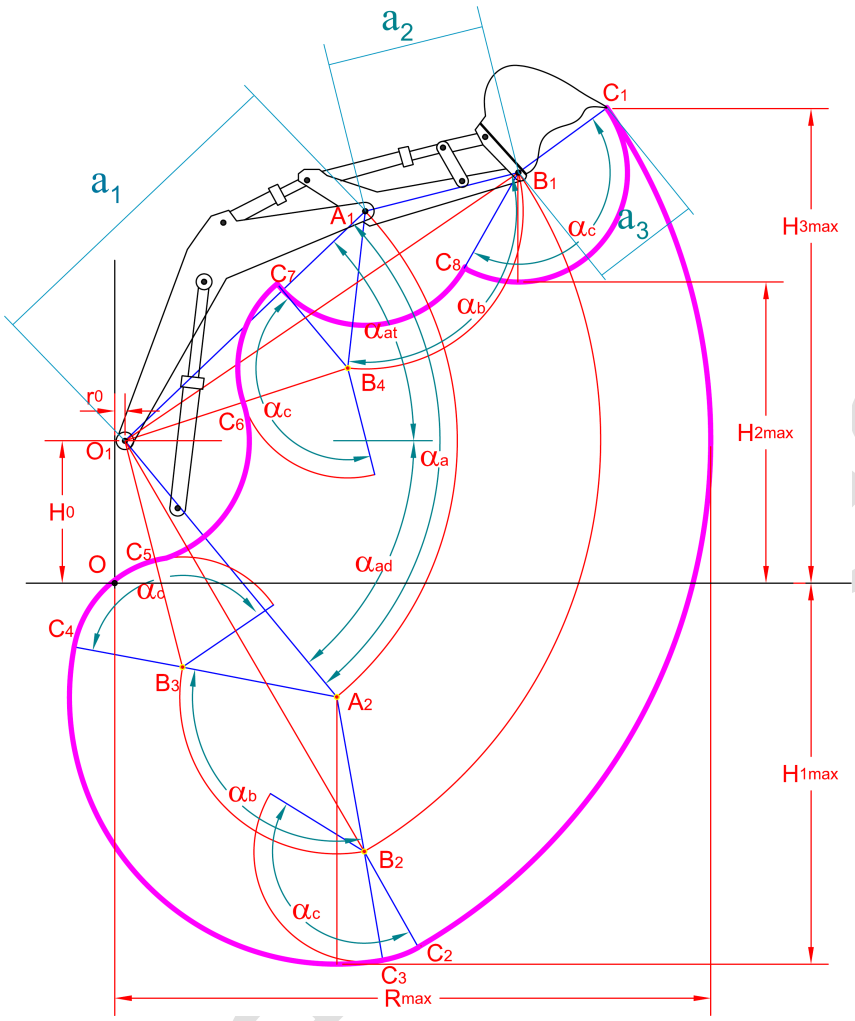


Fig. 1. Diagram for determining the working area of the bucket in backhoe excavators

hinge joints $\alpha_a(\alpha_{ad} + \alpha_{at})$, $\alpha_b$, $\alpha_c$, define the reach of the bucket tooth $C_1$. Depending on the machine's application and power, the equipment is designed with specific link lengths $a_1$, $a_2$, $a_3$, and the rotation angles are typically chosen as follows [19]: $\alpha_a = 40° \div 45°$, $\alpha_{ad} = 45° \div 55°$, $\alpha_b = 95° \div 115°$, $\alpha_c = 140° \div 160°$. The working area of the bucket (see Fig. 1, where point O denotes the intersection of the rotation axis with the vertical plane of the machine base, and point $O_1$ (the pivot joint of the boom base) is located at a horizontal distance of $r_0$ and a vertical height of $H_0$) is determined by adjusting the linkage dimensions within these defined rotation angles according to the machine operation principles.

The working area is determined through the following procedure: Initially, the boom cylinder is fully extended, while both the arm cylinder and bucket cylinder are fully retracted, positioning the bucket of the excavator at its maximum height, with the bucket teeth reaching their highest coordinate point (position $C_1$). The arc $C_1C_2$ is defined by fixing the arm cylinder and bucket cylinder, while fully retracting the boom cylinder, resulting in a circular arc centered at $O_1$ with a radius of $O_1C_1$ and an angle $\alpha_a$. The arc $C_2C_3$ is subsequently obtained by rotating the bucket around point $B_2$ until $A_2B_2$ aligns with $B_2C_2$, at which point $C_2$ intersects with $C_3$. The arc $C_3C_4$ is traced by rotating the arm exclusively, within the limited rotation angle $\alpha_b$. With the boom fixed at position $O_1A_2$ and the arm at position $A_2B_3$, the bucket is then rotated

Table 1. The relationship between the trajectory envelopes of the working paths and the range of variation in the rotation angles of the working equipment ($0 < \delta_1 < \delta_2 < 1$)

| Arc | $\alpha_a$ | $\alpha_b$ | $\alpha_c$ |
|---|---|---|---|
| 1 ($C_1C_2$) | $\left[\alpha_a^{\mathrm{U}}\alpha_a^{\mathrm{L}}\right]$ | $\alpha_b^{\mathrm{U}}$ | $\alpha_c^{\mathrm{U}}$ |
| 2 ($C_2C_3$) | $\alpha_a^{\mathrm{L}}$ | $\alpha_b^{\mathrm{U}}$ | $\left[\alpha_c^{\mathrm{U}}\delta_1\alpha_c^{\mathrm{L}}\right]$ |
| 3 ($C_3C_4$) | $\alpha_a^{\mathrm{L}}$ | $\left[\alpha_b^{\mathrm{U}}\alpha_b^{\mathrm{L}}\right]$ | $\delta_1\alpha_c^{\mathrm{L}}$ |
| 4 ($C_4C_5$) | $\alpha_a^{\mathrm{L}}$ | $\alpha_b^{\mathrm{L}}$ | $\left[\delta_1\alpha_c^{\mathrm{L}}\delta_2\alpha_c^{\mathrm{L}}\right]$ |
| 5 ($C_5C_6$) | $\left[\alpha_a^{\mathrm{L}}\alpha_a^{\mathrm{U}}\right]$ | $\alpha_b^{\mathrm{L}}$ | $\delta_2\alpha_c^{\mathrm{L}}$ |
| 6 ($C_6C_7$) | $\alpha_a^{\mathrm{U}}$ | $\alpha_b^{\mathrm{L}}$ | $\left[\delta_2\alpha_c^{\mathrm{L}}\alpha_c^{\mathrm{L}}\right]$ |
| 7 ($C_7C_8$) | $\alpha_a^{\mathrm{U}}$ | $\left[\alpha_b^{\mathrm{L}}\alpha_b^{\mathrm{U}}\right]$ | $\alpha_c^{\mathrm{L}}$ |
| 8 ($C_8C_1$) | $\alpha_a^{\mathrm{U}}$ | $\alpha_b^{\mathrm{U}}$ | $\left[\alpha_c^{\mathrm{L}}\alpha_c^{\mathrm{U}}\right]$ |

along the arc $B_3C_4$ until $C_4$ reaches $C_5$, where point $C_5$ is defined as the intersection of the bucket arc with segment $O_1B_3$. The boom cylinder is then fully extended to move the working attachment from position $A_2B_3C_5$ to position $A_1B_4C_6$, thereby delineating the arc $C_5C_6$. The arc $C_6C_7$ is formed by fully extending the bucket cylinder, followed by arc $C_7C_8$, obtained by fully retracting the arm cylinder. Finally, the arc $C_8C_1$ is traced by fully retracting the bucket cylinder. These arcs and the corresponding rotation angles are detailed in Table 1.

Consequently, using geometric methods, the reach range of the bucket teeth is determined as the closed curve $C_1C_2C_3C_4C_5C_6C_7C_8C_1$ which represents the working range of the original hydraulic backhoe excavator. Based on this, the important characteristic dimensions of the working range can be identified as follows: maximum reach radius $R_{\max}$, maximum digging depth $H_{1\max}$, maximum dumping height $H_{2\max}$, and maximum reach height $H_{3\max}$. To illustrate a specific working range of an excavator with a bucket, the calculation result with the Komatsu PC800-6 hydraulic excavator is shown in Fig. 2.

The drum cutter employed for maritime channel opening is specifically designed to fragment soil and rock from the seabed, facilitating the subsequent removal of material by pumping equipment. A prevalent design for this application is the drum cutter, as illustrated in Fig. 3. To enhance the reach of the drum cutter assembly, particularly for operations at greater depths, a two-section boom configuration is adopted for the excavator's working equipment. As depicted in Fig. 4, the selected base excavator is equipped with a two-section boom along with other essential working components. This configuration enables the excavator to operate autonomously in shallow water environments or be mounted on floating platforms to effectively perform maritime channel opening tasks. Consequently, the incorporation of the drum cutter onto a two-section boom excavator induces significant modifications to the working area. This is attributable to the expanded dimensions and the increased number of moving components associated with the new configuration.

## 3. Formulations for kinematic analysis of long-reach excavator

To determine the working area of the drum cutter, this study employs the DH transformation method [6] to analyze the relationship between the coordinates of the point of interest on the workpiece and the movements of the driving links. The positional relationship between successive links is characterized by joint parameters. In this spatial analysis, the position of the joint

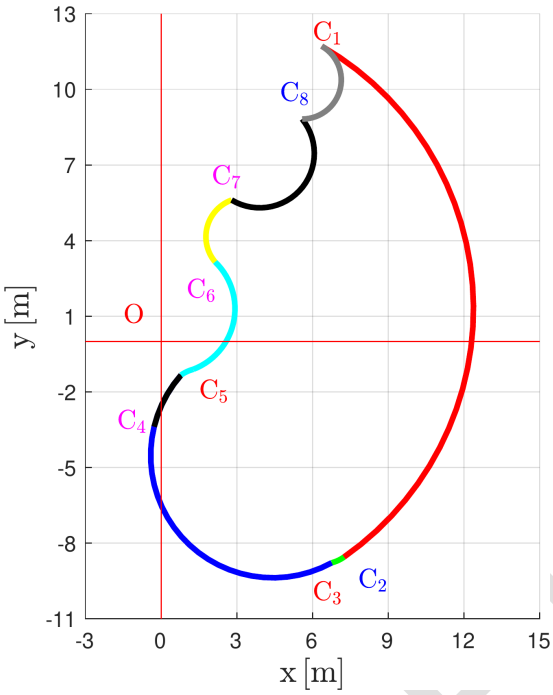


Fig. 2. Working area of the Komatsu PC800-6 hydraulic excavator with the original bucket

coordinate system $(\mathrm{O}xyz)_i$, relative to system $(\mathrm{O}xyz)_{i-1}$, is defined by four DH parameters: $\alpha_i$, $a_i$, $d_i$, and $q_i$.

To maintain generality, this study restricts analysis to the planar problem. The excavator system is modeled as comprising five rigid link units: chassis-cabin (link 0), boom (link 1), arm #1 (link 2), arm #2 (link 3), and drum cutter (link 4). The DH parameters of these links are listed in Table 2. These units are interconnected by hinge joints $\mathrm{O}_{i-1}$. The fixed coordinate system $\mathrm{O}_0x_0y_0z_0$ is positioned at the axis of rotation of the floor. Coordinate systems $\mathrm{O}_1x_1y_1z_1$,

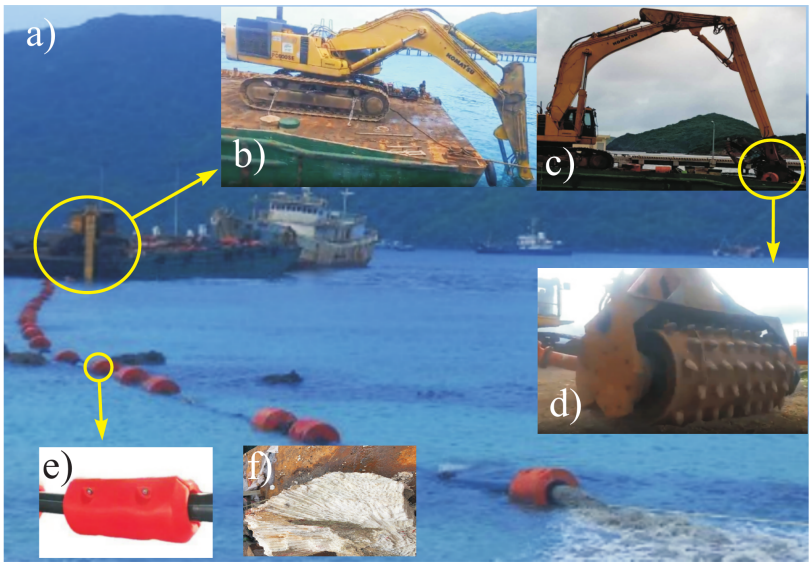


Fig. 3. Excavator with integrated drum cutter at construction site: (a) long-reach excavator equipped with a drum cutter for dredging, (b)–(c) close-up view, (d) drum cutter, (e) floating pipe, and (f) real cut-mark

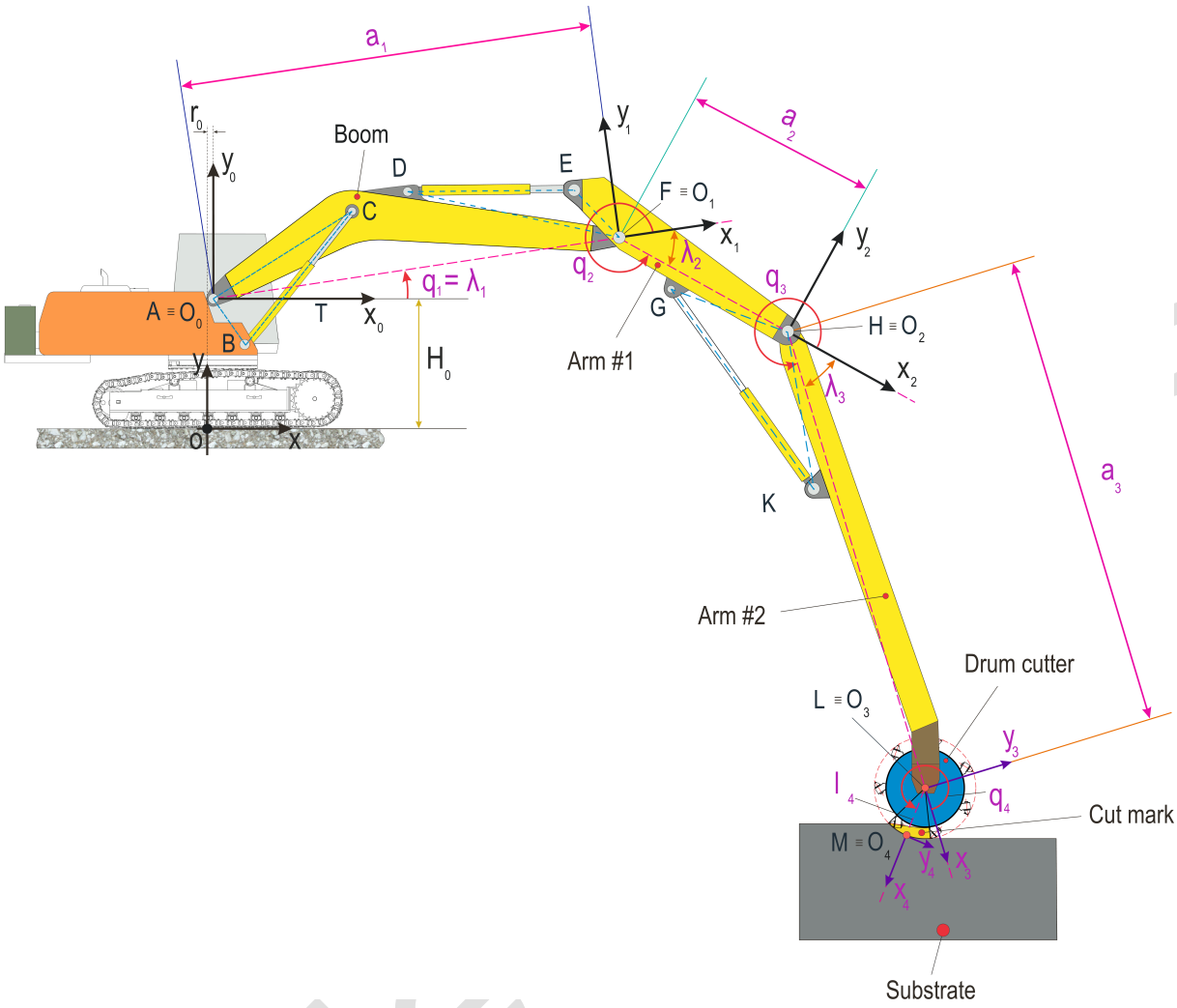


Fig. 4. Diagram for determining the working area of a drum cutter

Table 2. DH parameters of the dredging excavator

| Link $i$ | $\alpha_i$ | $a_i$ | $d_i$ | $q_i$ |
|---|---|---|---|---|
| 1 | 0 | $a_1$ | 0 | $q_1$ |
| 2 | 0 | $a_2$ | 0 | $q_2$ |
| 3 | 0 | $a_3$ | 0 | $q_3$ |
| 4 | 0 | $a_4$ | 0 | $q_4$ |

$O_2x_2y_2z_2$, $O_3x_3y_3z_3$, and $O_4x_4y_4z_4$ are defined at the attachment points between the machine and the drum cutter.

The DH matrix describes the relative position between link $(i)$ and link $(i-1)$:

$$D_{i-1}^{i} = \begin{bmatrix} \cos q_i & -\cos\alpha_i \sin q_i & \sin\alpha_i \sin q_i & a_i \cos q_i \\ \sin q_i & \cos\alpha_i \cos q_i & -\sin\alpha_i \cos q_i & a_i \sin q_i \\ 0 & \sin\alpha_i & \cos\alpha_i & d_i \\ 0 & 0 & 0 & 1 \end{bmatrix}, \; i = 1, 2, 3, 4. \tag{1}$$

The transformation matrix of the $k$-th link with the fixed coordinates is calculated as

$$D_0^k = \prod_{i=1}^{k} D_{i-1}^i = \begin{bmatrix} c_{1\ldots k} & -s_{1\ldots k} & 0 & a_1c_1 + \ldots + a_kc_{1\ldots k} \\ s_{1\ldots k} & c_{1\ldots k} & 0 & a_1s_1 + \ldots + a_ks_{1\ldots k} \\ 0 & 0 & 1 & 0 \\ 0 & 0 & 0 & 1 \end{bmatrix}, \tag{2}$$

where $c_{1\ldots k} = \cos(q_1 + \ldots + q_k)$ and $s_{1\ldots k} = \sin(q_1 + \ldots + q_k)$. Therefore, the coordinates of the drum cutter center are calculated as follows:

$$\begin{bmatrix} x_{\mathrm{O}_3} \\ y_{\mathrm{O}_3} \end{bmatrix} = \begin{bmatrix} r_0 + a_1c_1 + \ldots + a_3c_{123} \\ H_0 + a_1s_1 + \ldots + a_3s_{123} \end{bmatrix}. \tag{3}$$

Therein, $r_0 = 0.45$ m is the distance between the $\mathrm{O}_y$ and $\mathrm{O}_{y_1}$ axes (i.e., horizontal distance from the working machine platform to the pivot axis of the boom joint), $H_0 = 2.254$ m is the distance between the $\mathrm{O}_x$ and $\mathrm{O}_{x_1}$ axes (i.e., vertical distance from the working machine platform to the pivot axis of the boom joint). Point O represents the intersection of the line passing through the center of rotation of the machine platform and the vertical axis of the machine base. Point $\mathrm{O}_1$ denotes the swing joint at the boom.

By analyzing the limited values of $q_i$, the working area of the drum cutter can be determined using a method analogous to the diagram presented in Fig. 1. As illustrated in Fig. 4, the lifting and movements of the boom, arm #1, and arm #2 are each controlled by their respective hydraulic cylinders. Consequently, the length of these hydraulic cylinders is directly related to the joint angles of the corresponding components. Variations in these angles subsequently lead to changes in the position of the drum cutter. As shown in Fig. 5, the relationships between the joint angles and the hydraulic cylinders are calculated using geometric methods as follows [35, 39]:

*Boom cylinder:* According to the geometrical relationship of boom structure in Fig. 5, the relationship between $l_{\mathrm{BC}}$ and $\lambda_1$ can be expressed as

$$\begin{aligned} &\overline{\mathrm{BC}} = \overline{\mathrm{B_0C_0}} + V_1t, \\ &\lambda_1 = q_1 = \arccos\left(\frac{\overline{\mathrm{AB}}^2 + \overline{\mathrm{AC}}^2 - \overline{\mathrm{BC}}^2}{2\,\overline{\mathrm{AB}}\,\overline{\mathrm{AC}}}\right) - \angle\mathrm{TAB} - \angle\mathrm{CAF}. \end{aligned} \tag{4}$$

*Arm #1 cylinder:* According to the geometrical relationship of the arm #1 structure in Fig. 5, the relationship between $l_{\mathrm{DE}}$ and $\lambda_2$ can be expressed by

$$\begin{aligned} &\overline{\mathrm{DE}} = \overline{\mathrm{D_0E_0}} + V_2t, \\ &\lambda_2 = 2\pi - q_2 = \angle\mathrm{HFE} - \pi + \arccos\left(\frac{\overline{\mathrm{DF}}^2 + \overline{\mathrm{EF}}^2 - \overline{\mathrm{DE}}^2}{2\,\overline{\mathrm{DF}}\,\overline{\mathrm{EF}}}\right) + \angle\mathrm{DFA}. \end{aligned} \tag{5}$$

*Arm #2 cylinder:* According to the geometrical relationship of the arm #2 structure in Fig. 5, the relationship between $l_{\mathrm{GK}}$ and $\lambda_3$ can be given as

$$\begin{aligned} &\overline{\mathrm{GK}} = \overline{\mathrm{G_0K_0}} + V_3t, \\ &\lambda_3 = 2\pi - q_3 = \pi - \angle\mathrm{KHL} - \angle\mathrm{FHG} - \arccos\left(\frac{\overline{\mathrm{GH}}^2 + \overline{\mathrm{HK}}^2 - \overline{\mathrm{GK}}^2}{2\,\overline{\mathrm{GH}}\,\overline{\mathrm{HK}}}\right). \end{aligned} \tag{6}$$

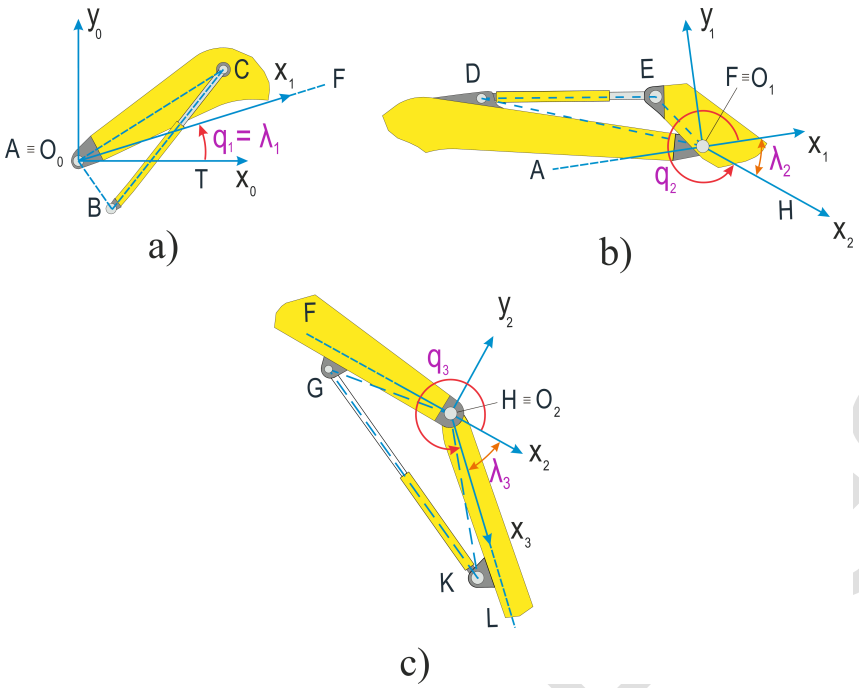


Fig. 5. Schematic diagram of the long-reach excavator equipped with attached drum cutter: (a) boom cylinder driving loop, (b) arm #1 cylinder driving loop, (c) arm #2 cylinder driving loop

In (4)–(6), the subscript "0" denotes the cylinder length at the time $t = 0$, and $V_{1,2,3}$ are respectively the extended speeds of the boom, arm #1 cylinder, and arm #2 cylinder.

The objective of the kinematic study presented in this paper is to establish the relationship between the displacement of the driving cylinders and the rotation angles of the boom, arm #1, and arm #2. By understanding these relationships, the kinematic characteristics related to the drum cutter center can be calculated through (3). By differentiating the position vector of the center of drum cutter, given in (3), with respect to time, we obtain the velocity vector as follows:

$$\begin{bmatrix} V_{dx} \\ V_{dy} \end{bmatrix} = \begin{bmatrix} \dot{x}_{O_3} \\ \dot{y}_{O_3} \end{bmatrix} = \begin{bmatrix} -a_1\dot{q}_1 s_1 - a_2\dot{q}_{12}s_{12} - a_3\dot{q}_{123}s_{123} \\ a_1\dot{q}_1 c_1 + a_2\dot{q}_{12}c_{12} + a_3\dot{q}_{123}c_{123} \end{bmatrix}. \tag{7}$$

Then, the absolute velocity of the drum cutter center can be calculated using the following expression:

$$V_d = \sqrt{V_{dx}^2 + V_{dy}^2}. \tag{8}$$

## 4. Dynamic model of backhoe dredger

In construction machinery design, particularly for hydraulic excavators, dynamic analysis of the working process plays a crucial role in assessing system performance, operational stability, and structural durability. Several approaches have been traditionally employed to study the dynamics of such systems. These approaches encompass theoretical calculations derived from simplified mathematical models, experimental investigations carried out on physical prototypes or scaled models, and numerical simulations conducted with computer-aided engineering software. Among the available simulation packages, Adams package stands out as one of the most powerful and widely adopted software packages for multibody dynamics analysis [25,30].

Adams enables the construction of kinematic and dynamic models of hydraulic excavators, representing the boom, arm, bucket, undercarriage, and hydraulic actuators as interconnected rigid or flexible bodies. The software is capable of computing displacements, velocities, accelerations, joint forces, and moments under realistic operating cycles.

### *4.1. Cutting model*

The drum cutter removes materials from the substrate through a set of cutting teeth arranged around its rotating drum surface. As the cutting power represents a major component of the total energy consumption, the design and selection of the drum cutter are critical factors affecting the system's operational performance and energy efficiency. The cutting model, shown in Fig. 6, is used to calculate the components of the cutting resistance forces for solving the dynamic model of the equipment.

The instantaneous cutting thickness corresponding to the $i$-th tooth at a given cutting angle, defined by $\Omega_i(t) = \omega t + \varphi_i$, can be expressed [23, 37]:

$$h_i(t) = \begin{cases} \dfrac{60V_d}{n_r m} \sin\Omega_i & \text{for } \mathrm{mod}(\Omega_i, 2\pi) \leq \alpha, \\ 0 & \text{otherwise,} \end{cases} \tag{9}$$

where $\omega = \pi n_r/30$ denotes the rotational speed of the drum cutter, $V_d$ is the translational velocity, $\alpha$ represents the contact angle corresponding to the number of engaged cutting picks, $d$ is the cutting depth, $R$ is the drum cutter radius, $\varphi_i$ indicates the initial engagement phase of the $i$-th pick, and $m$ denotes the total number of picks distributed along the cutting path.

For an individual pick along the cutting line, the cutting force $F_{ci}$ and the normal force $F_{ni}$ can be determined according to the theoretical model proposed by Goktan [10, 12]

$$F_{ci} = \frac{4\pi\sigma_t h_i^2 \sin^2(\theta+\psi)}{\cos(\theta+\psi)}, \qquad F_{ni} = \frac{2F_{ci}}{\tan\left(\frac{\pi}{2} - \theta + \psi\right)}, \tag{10}$$

where $\sigma_t$ is the unconfined compressive strength of the rock, $\theta$ is the semi-angle of conical pick, and $\psi$ is the friction angle between the pick and rock.

The total cutting force, comprising both horizontal and vertical components, is estimated based on the number of picks $n_c$ simultaneously interacting with the rock by the following

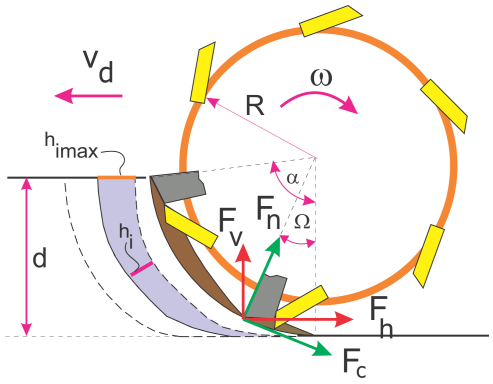


Fig. 6. Diagram of the cutting process of drum cutter

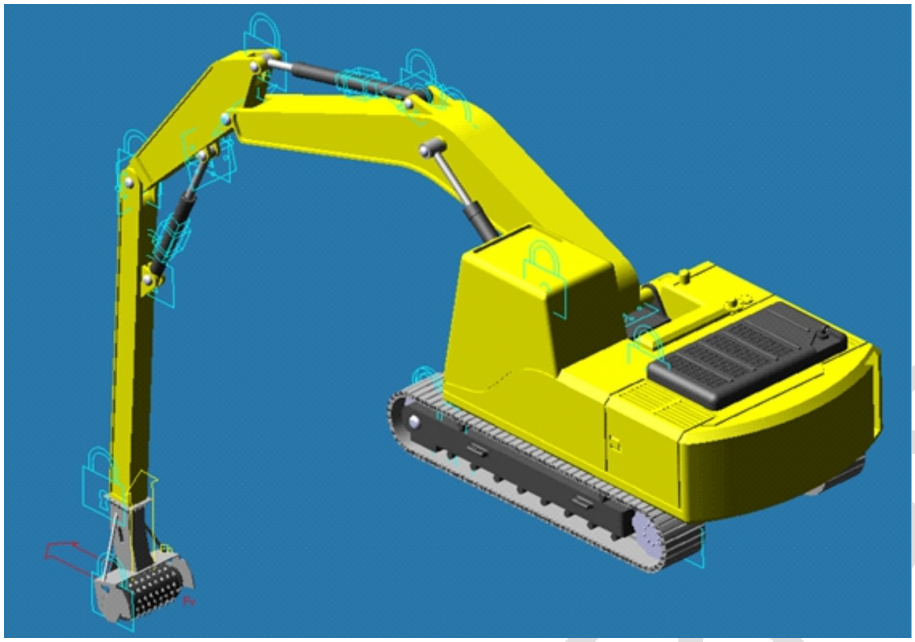

Fig. 7. Model of the long-reach excavator with drum cutter in Adams

expressions [8, 33]:

$$F_h = \sum_{i=1}^{n_c} F_{ci} \cos \Omega_i + F_{ni} \sin \Omega_i, \qquad F_v = \sum_{i=1}^{n_c} -F_{ci} \sin \Omega_i + F_{ni} \cos \Omega_i. \tag{11}$$

### *4.2. Dynamic model*

The 3D geometry model of the hydraulic excavator and its components were first developed in Autodesk Inventor. The detailed models included the complete excavator assembly within the drum cutter. These models provided a precise geometric basis for building the dynamic simulation. The geometry assembly was then imported into Adams for further processing. The working environment is defined by setting the unit system, gravity, and working grid to replicate real operating conditions. Subsequently, kinematic pairs are established at the joints, including fixed pair between the base and the ground, revolute joints for rotational connections, and translational joints between each hydraulic cylinder and its piston rod, as shown in Fig. 7. After the linkage of components, several input parameters related to the motion of the driving cylinders and the resistance forces acting on the drum cutter are assigned to the objects according to the scenario, in order to analyze the kinematic and dynamic responses of the system (see Section 5.3).

## 5. Results and discussion

### *5.1. Assessments of working area of drum cutter mounted on long-reach excavator*

Using the construction method for the working area described above and employing Matlab software to solve the problems outlined in Section 3. Fig. 8 depicts the working area of the drum cutter integrated into the original Komatsu PC800-6 excavator across three different structural configurations, with the following sections providing detailed explanations of the primary aspects:

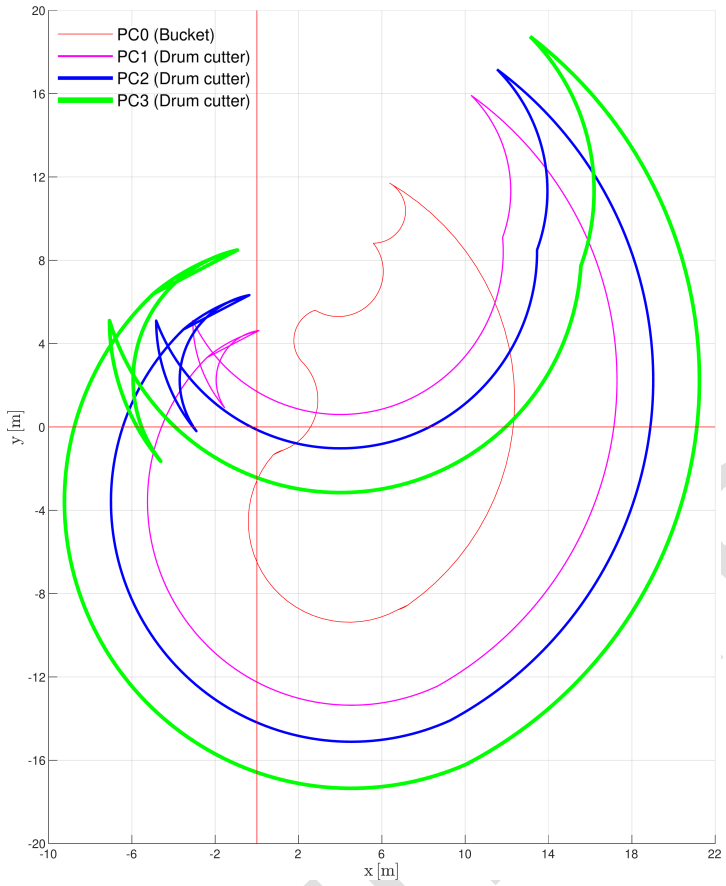


Fig. 8. The working area of bucket (PC0) and drum cutter with three different configurations (PC1, PC2, PC3)

(i) Given the structure and dimensions of the replacement part depicted in Fig. 4, the survey results of the working areas for the drum cutter mounted on the excavator and the original bucket reveal significant differences in both shape and magnitude. Specifically, in case (PC2), when replacing the arm #2 with a new length of $a_3 = 8.242\,\text{m}$ and altering the structural angle, the working area of the drum cutter mounted on the excavator expands downward (relative to the vertical plane of the machine), resulting in an increase of approximately $2.35$ times compared to the original bucket.

(ii) In cases of changing the length of arm #2, the resulting working areas are illustrated in Fig. 9a–c (PC1 and PC3). Specifically, when the length of arm #2 ($a_3$) is adjusted from $8.242\,\text{m}$ to $10.500\,\text{m}$, the working area increases by approximately $1.21$ times.

Table 3 provides information on key dimensions, including $R_{\max}$, $H_{1\max}$, $H_{3\max}$ and the working areas (as depicted in Fig. 1) of both the bucket and the drum cutters. The analysis reveals that the working area of the bucket mounted on the original excavator is markedly smaller compared to that of the drum cutter installed on the same model of excavator with the newly replaced arm #2. This discrepancy becomes particularly evident in regions where the depth exceeds $5\,\text{m}$. The data clearly indicate that integrating the drum cutter with the extended arm segment on the original excavator not only significantly enhances the depth of reach but also substantially enlarges the downward working area. Therefore, this modification considerably improves the excavator's capacity to undertake channel excavation tasks under specific conditions.

Table 3. Typical dimensions of the working area for bucket and drum cutters

| Parameter | | Bucket | | Drum cutter | |
|---|---|---|---|---|---|
| | | PC0 | PC1 | PC2 | PC3 |
| | | $a_3 = 1.550\,\mathrm{m}$ | $a_3 = 6.500\,\mathrm{m}$ | $a_3 = 8.242\,\mathrm{m}$ | $a_3 = 10.500\,\mathrm{m}$ |
| $R_{\max}$ [m] | | 12.37 | 17.29 | 19.03 | 21.25 |
| $H_{1\max}$ [m] | | 9.37 | 13.36 | 15.11 | 17.35 |
| $H_{3\max}$ [m] | | 11.71 | 15.92 | 17.17 | 18.75 |
| Total working area [$m^2$] | | 164.57 | 324.95 | 387.05 | 466.47 |
| Working area [$m^2$] | depth $< 0\,\mathrm{m}$ | 90.41 | 234.05 | 300.91 | 378.96 |
| | depth $< 5\,\mathrm{m}$ | 34.38 | 125.98 | 180.78 | 264.66 |
| | depth $< 10\,\mathrm{m}$ | 0 | 34.24 | 68.90 | 128.04 |

### *5.2. Kinematic analysis*

Based on the calculation diagram presented in Fig. 4, the input data set for the analysis is determined as follows: $\overline{\mathrm{AB}} = 0.979\,\mathrm{m}$, $\overline{\mathrm{AC}} = 2.845\,\mathrm{m}$, $\overline{\mathrm{EF}} = 1.113\,\mathrm{m}$, $\overline{\mathrm{DF}} = 3.758\,\mathrm{m}$, $\overline{\mathrm{GH}} = 2.154\,\mathrm{m}$, $\overline{\mathrm{KH}} = 2.742\,\mathrm{m}$, $\overline{\mathrm{B_0C_0}} = 2.968\,\mathrm{m}$, $\overline{\mathrm{D_0E_0}} = 2.898\,\mathrm{m}$, $\overline{\mathrm{G_0K_0}} = 4.254\,\mathrm{m}$, $\angle\mathrm{TAB} = 55.07°$, $\angle\mathrm{CAF} = 23.67°$, $\angle\mathrm{HFE} = 163.34°$, $\angle\mathrm{KHL} = 7.37°$, $\angle\mathrm{FHG} = 9.51°$, $\angle\mathrm{DFA} = 21.17°$. Fig. 9 illustrates the relationship between time and the velocities of the drum cutter center, including velocities in the $x$- and $y$-directions as well as the absolute velocity. This analysis is conducted under three distinct scenarios: the drum cutter is driven by the displacement of cylinder boom (Fig. 9a), the drum cutter is driven by the displacement of arm #1 cylinder (Fig. 9b), the drum cutter is driven by the displacement of arm #2 cylinder (Fig. 9c) and position of the drum cutter center in the three cases (Fig. 9d).

Another survey result is also presented and illustrated in Fig. 10. This result is conducted under three distinct scenarios: the drum cutter is driven by the displacement of cylinder boom (Fig. 10a), the drum cutter is driven by the combined displacement of the boom cylinder and arm #1 cylinder (Fig. 10b), the drum cutter is driven by the displacement of all three cylinders (Fig. 10c) and position of the drum cutter center in the three cases (Fig. 10d).

For each scenario, the displacement speed of all cylinders is set to $0.3\,\mathrm{m\,min^{-1}}$. The results, presented in Figs. 9 and 10, illustrate the velocity trends and highlight the influence of the driving cylinder displacements on the drum cutter velocity. Specifically, for a given cylinder movement speed, the velocity components of the drum cutter vary throughout the cutting process. The cutting velocity in each direction depends on the position of the drum cutter, leading to different values in the vertical and horizontal directions. In the surveyed cutting trajectory (located along the $\mathrm{C_1C_2}$ arc as shown in Fig. 2), the vertical cutting speed $V_{dy}$ is generally greater than the horizontal cutting speed $V_{dx}$. The results indicate that the working area of the cutting head significantly influences the characteristics of these velocity variations.

To examine the dependence of cylinder feed rates and cutting methods (based on cylinder displacement control), the results in Fig. 11 have been extended to cover a working speed range for the cylinders from $0.1\,\mathrm{m\,min^{-1}}$ to $0.5\,\mathrm{m\,min^{-1}}$. The subsequent section, presented in Fig. 11, will detail the average velocity value $V_{dx}^{\mathrm{ave}}$, as well as the maximum $V_d^{\max}$ and minimum $V_d^{\min}$ ones.

Fig. 11 illustrates the relationship between the displacement velocity of the cylinders and the velocity of the drum cutter for seven scenarios—individual operation of each cylinder and

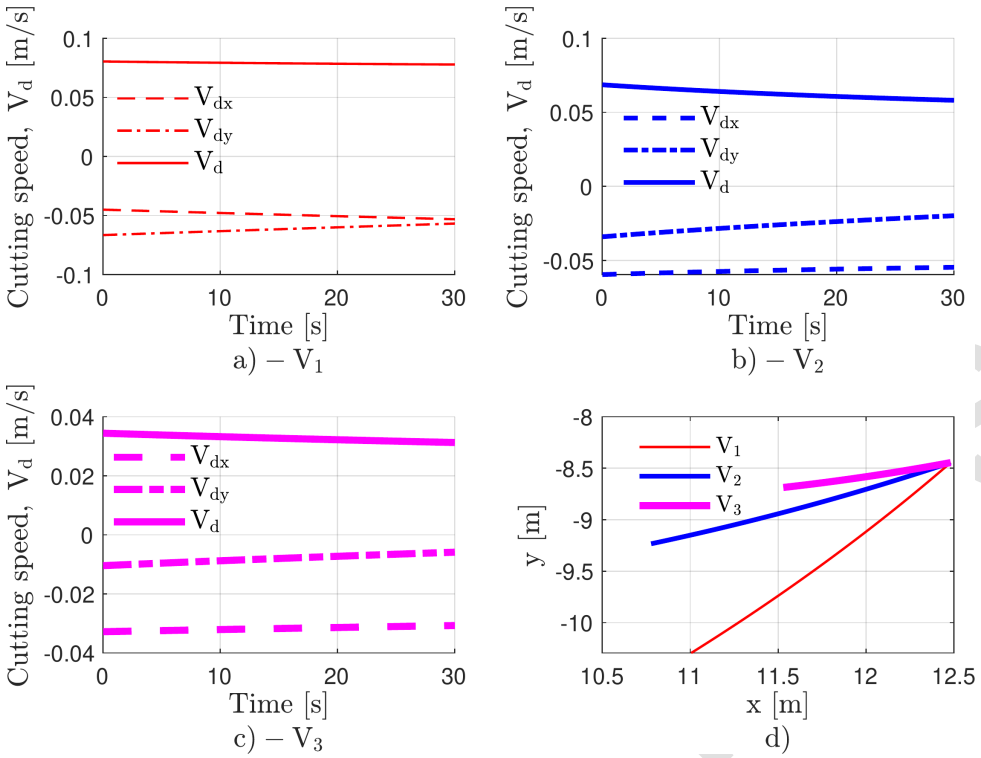


Fig. 9. Time-dependent velocity of the drum cutter center: (a) case of operating boom cylinder, (b) case of operating arm #1 cylinder, (c) case of operating arm #2 cylinder, and (d) position of the drum cutter center

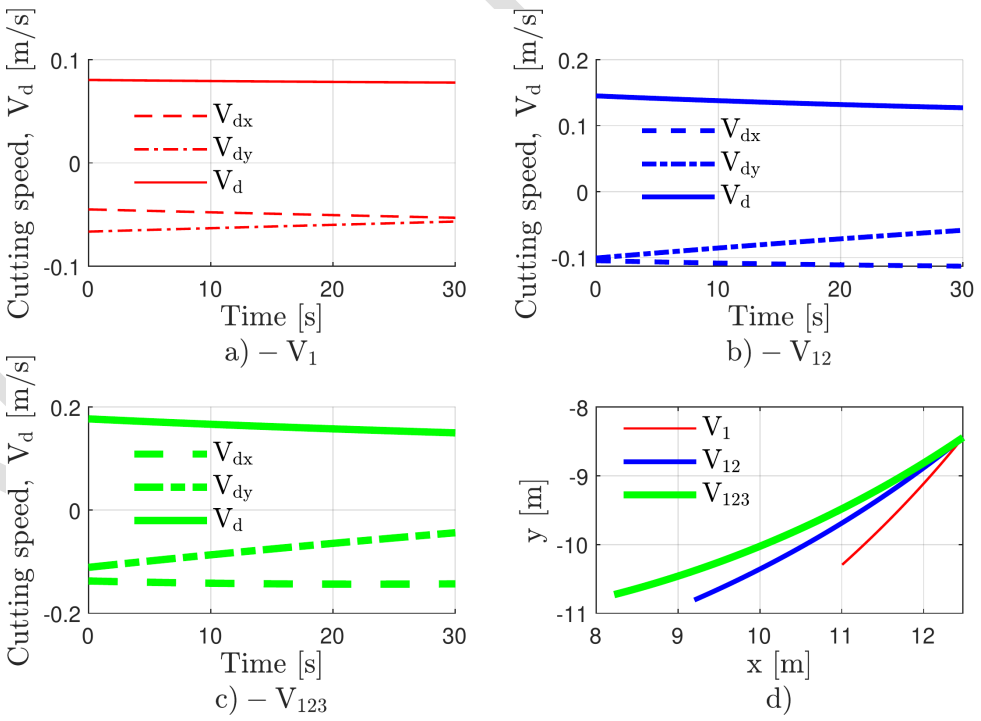


Fig. 10. Time-dependent velocity of the drum cutter center: (a) case of operating boom cylinder, (b) case of operating cylinder of boom and arm #1, (c) case of operating all cylinders, (d) position of the drum cutter center

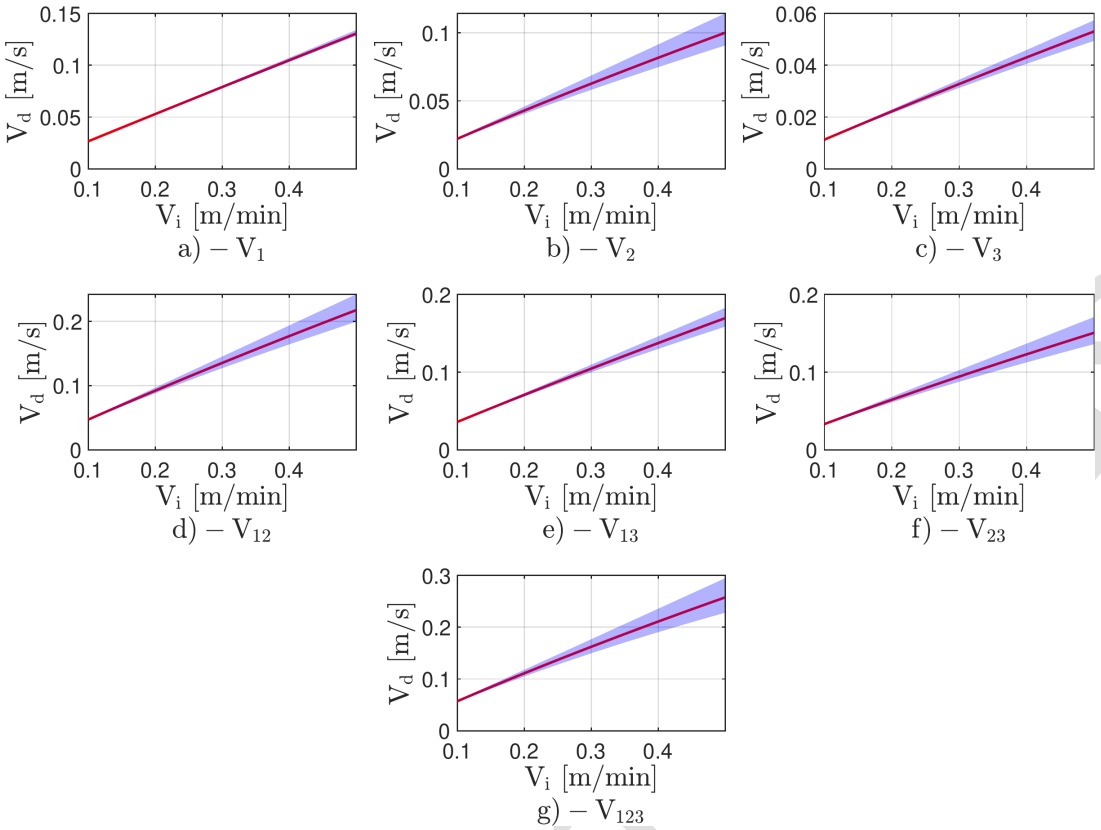


Fig. 11. Graph illustrating the relationship between the displacement velocities of the cylinders and the velocity of the drum cutter: (a)–(c) cases in which each cylinder ($VC_1$, $VC_2$, $VC_3$) operates individually, (d)–(f) pairs of cylinders ($VC_{12}$, $VC_{13}$, $VC_{23}$) operate together, and (g) all three cylinders ($VC_{123}$) operate together

combined operation of two or three cylinders, specifically:

(i) Based on the data illustrated in Fig. 11a–c, it is evident that the displacement of the boom cylinder exerts the most significant influence on the displacement of the drum cutter. Specifically, the velocity of the drum cutter's movement is approximately 16 times greater than that of the boom cylinder. Following this, the displacements of the arm #1 and arm #2 cylinders also contribute notably to the drum cutter's movement, with amplification factors of approximately 12 and 6 times, respectively.

(ii) Fig. 11d–g illustrates that the drum cutter reaches its maximum displacement velocity when all three cylinders operate simultaneously. In scenarios with combinations of any two cylinders, the displacement velocity of the drum cutter remains relatively high. These results further underscore the critical role of the boom cylinder's movement in enhancing the displacement velocity of the drum cutter.

Table 4 presents the effect of each cylinder's displacement speed on the drum cutter velocity. When the drum cutter is operated by the individual displacement of each cylinder (i.e., boom, arm #1, and arm #2), the velocity ratio of the drum cutter relative to the cylinder is maximized at approximately 15.734 when the boom cylinder functions at a speed of 0.1 m min$^{-1}$. Similarly, when the drum cutter is driven by the combined displacements of two or all three cylinders, the maximum velocity ratio is approximately 33.996 when all three cylinders are operating at a speed of 0.1 m min$^{-1}$.

Table 4. Velocity values of the cylinders and drum cutter

| Case | $V_i\,[\mathrm{m\,min^{-1}}]$ | $V_d^{\min}\,[\mathrm{m\,s^{-1}}]$ | $V_d^{\max}\,[\mathrm{m\,s^{-1}}]$ | $V_d^{\mathrm{ave}}\,[\mathrm{m\,s^{-1}}]$ | $\frac{V_d^{\max}-V_d^{\min}}{V_d^{\mathrm{ave}}}$ | $\frac{V_d^{\mathrm{ave}}}{V_i}$ |
|---|---|---|---|---|---|---|
| $VC_1$ | 0.1 | 0.0261 | 0.0264 | 0.0262 | 0.0132 | 15.7340 |
| | 0.5 | 0.1266 | 0.1320 | 0.1287 | 0.0417 | 15.4390 |
| $VC_2$ | 0.1 | 0.0215 | 0.0232 | 0.0223 | 0.0728 | 13.3909 |
| | 0.5 | 0.0907 | 0.1159 | 0.1006 | 0.2506 | 12.0690 |
| $VC_3$ | 0.1 | 0.0109 | 0.0113 | 0.0111 | 0.0336 | 6.6799 |
| | 0.5 | 0.0489 | 0.0566 | 0.0525 | 0.1464 | 6.2948 |
| $VC_{12}$ | 0.1 | 0.0457 | 0.0482 | 0.0469 | 0.0546 | 28.1350 |
| | 0.5 | 0.1967 | 0.2411 | 0.2154 | 0.2062 | 25.8491 |
| $VC_{13}$ | 0.1 | 0.0347 | 0.0359 | 0.0353 | 0.0329 | 21.1584 |
| | 0.5 | 0.1556 | 0.1793 | 0.1664 | 0.1426 | 19.9636 |
| $VC_{23}$ | 0.1 | 0.0322 | 0.0343 | 0.0332 | 0.0650 | 19.9093 |
| | 0.5 | 0.1352 | 0.1715 | 0.1503 | 0.2416 | 18.0346 |
| $VC_{123}$ | 0.1 | 0.0549 | 0.0585 | 0.0567 | 0.0640 | 33.9961 |
| | 0.5 | 0.2242 | 0.2927 | 0.2544 | 0.2691 | 30.5310 |

### *5.3. Dynamic response*

For a given drum cutter configuration, characterized by parameters such as: $R = 0.5\,\mathrm{m}$, $\theta = 40^\circ$, $\psi = 10^\circ$, $\sigma_t = 21\,\mathrm{MPa}$, and $m = 8$. The investigation was carried out under the operating mode: $v_t = 0.05\,\mathrm{m\,s^{-1}}$, $n_r = 25\,\mathrm{rpm}$. When the cutting depth was varied at different values, the corresponding components of cutting resistance in both longitudinal and transverse directions were obtained. These resistance parameters, once determined, were incorporated into the Adams model to conduct dynamic simulations. For different cutting conditions, three types of curves illustrating the variation of cutting forces are presented in Fig. 12 for two cutting depths: $d_1 = 0.10\,\mathrm{m}$ (thick lines), and $d_2 = 0.15\,\mathrm{m}$ (thin lines). In details, the mean values (standard deviations) of cutting forces $F_h$ and $F_v$ are respectively as follows for the cutting depth $d_1$: 2.55 (0.83) and 2.84 (0.91), and for $d_2$: 9.27 (2.10) and 10.14 (2.27), with units in kN. The obtained results indicate a significant influence of the cutting depth on variations of the resistance force components.

With the scope limited to studying the dynamic characteristics within the operating plane of the working equipment (while the swing mechanism is not operating). By incorporating the two cases of resistance forces presented in Fig. 12 and the dynamic model, the system responses can be obtained. Note that the actuation speed of the cylinders is selected so that the cutting head's motion velocity matches the value used in the cutting resistance model calculations. As shown in Fig. 13, the variation of the required actuation force in the working cylinders can be observed. It shows that, to overcome the resistance during operation, the changes in the actuation force follow the variations of the cutting forces. Some statistical parameters of the actuation forces are estimated in Table 5.

From the perspective of the machine working capability, for boom cylinders with rod piston/cylinder diameters of $140/200\,\mathrm{mm}$, operating at a working pressure of $31.4\,\mathrm{MPa}$, it can be readily observed that the maximum achievable force is approximately $503.1/986.5\,\mathrm{kN}$. This value is significantly higher than the maximum required boom driving force, $F_{B,\max} = 299.3\,\mathrm{kN}$

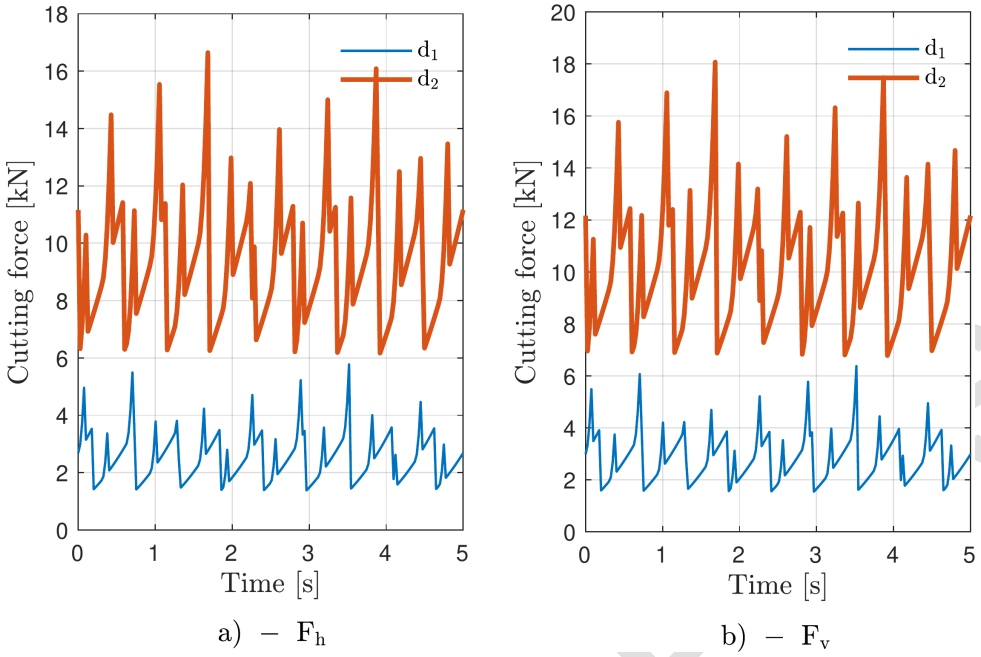


Fig. 12. Variation of the cutting resistance components over time corresponding to two cutting depths: (a) horizontal and (b) vertical components of the resistance force

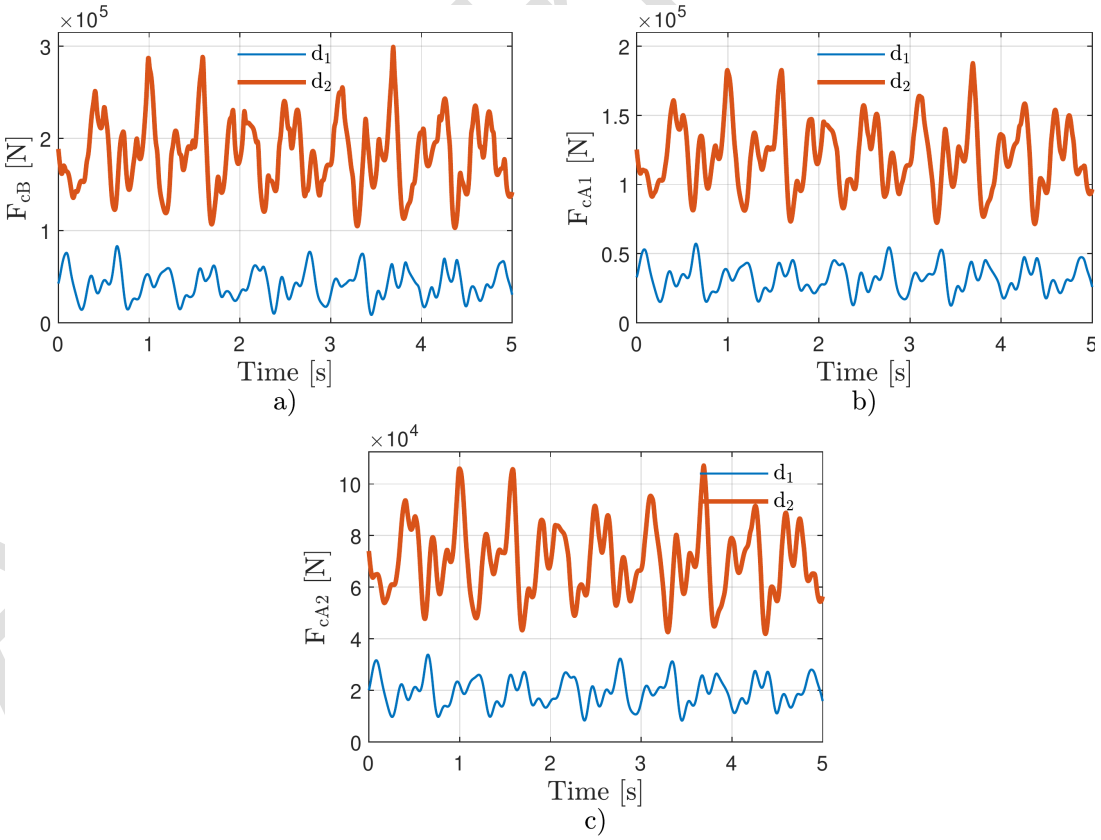


Fig. 13. Variation in the driving force of (a) the boom cylinder $F_{cB}$, (b) the arm #1 cylinder $F_{cA1}$, and (c) the arm #2 cylinder $F_{cA2}$

Table 5. Statistical parameters of the actuation forces

| | $F_{cB}$ [kN] | | $F_{cA1}$ [kN] | | $F_{cA2}$ [kN] | |
|---|---|---|---|---|---|---|
| cutting depth | Mean | Standard deviation | Mean | Standard deviation | Mean | Standard deviation |
| $d_1$ | 41.8 | 15.5 | 32.2 | 9.6 | 19.5 | 5.5 |
| $d_2$ | 181.9 | 38.7 | 120.1 | 24.1 | 70.0 | 13.9 |

(see Fig. 13a). Similarly, the values of $488.9/844.0$ kN represent the working capacity of the cylinder arm #1 (with piston rod/cylinder diameters of $120/185$ mm), whereas the maximum acting force is $F_{cA1,\max} = 187.8$ kN (see Fig. 13b).

In the dynamic calculation model, the reaction forces at the joints are also essential parameters to be determined. Fig. 14 illustrates the variations of the reaction forces in the vertical (dashed lines) and horizontal (solid lines) directions at the three main joints (A: boom-upper frame joint, F: boom-arm joint, and H: joint between the two arms). Similarly to the actuation forces, the joint reaction forces also reveal the influence of the cutting resistance factors. The results of the joint reaction forces indicate that, at joint A, the two components are relatively balanced in both directions. In contrast, the other two joints exhibit clear differences between the two directions: joint F mainly experiences horizontal reaction forces, whereas joint H shows a dominant vertical component.

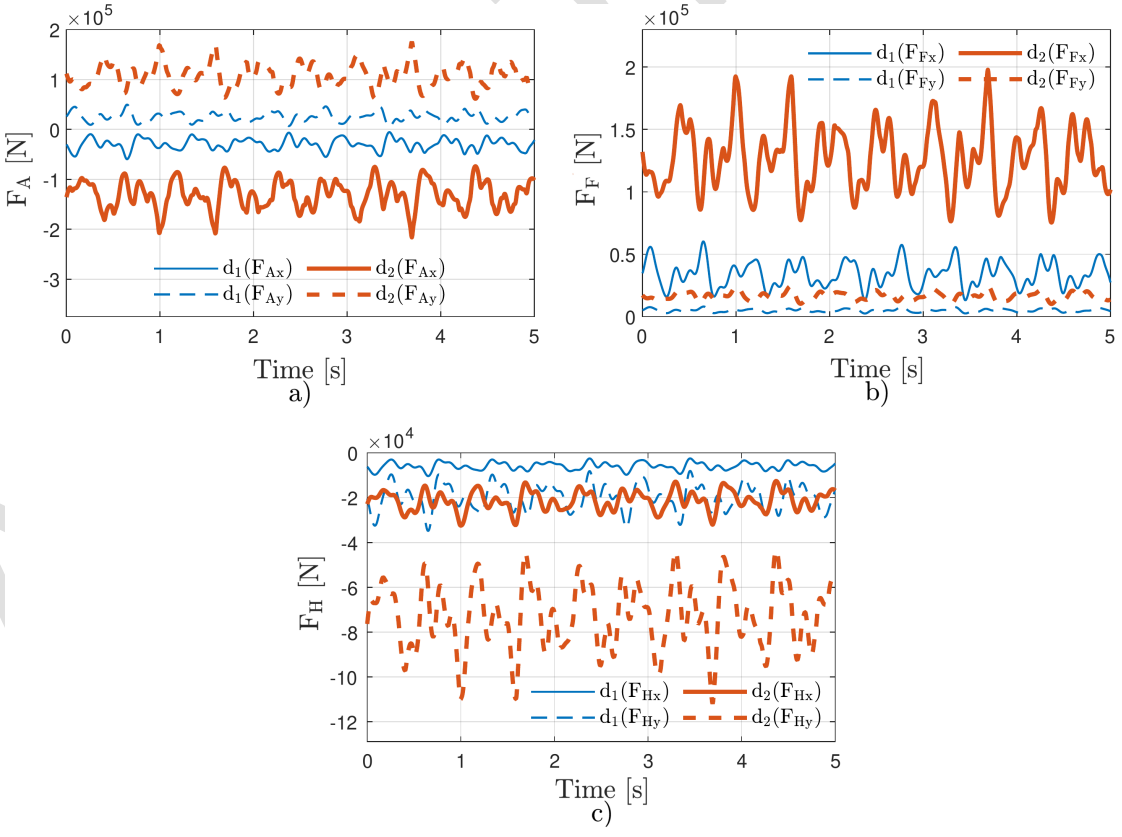


Fig. 14. Forces in the three joints of the working equipment – results presented with solid and dashed lines corresponding to the horizontal and vertical reaction forces

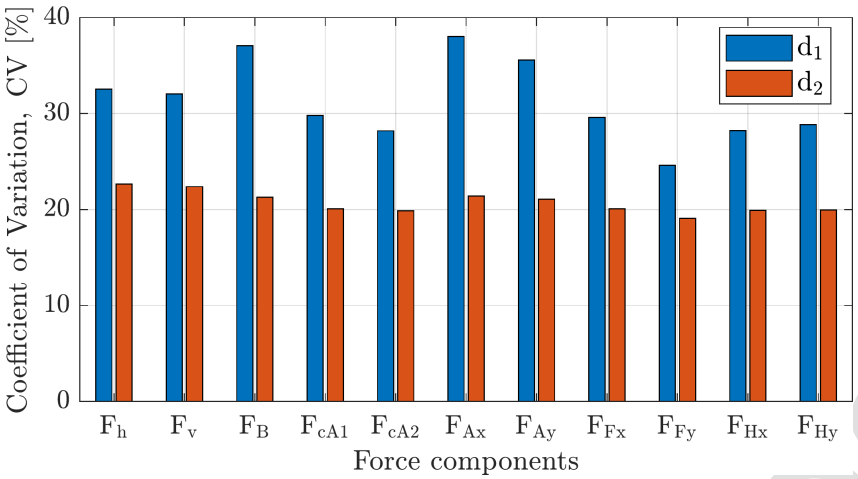


Fig. 15. Coefficient of variation of the force components for two cutting depths

Fig. 15 presents the coefficient of variation (CV), defined as the ratio of the standard deviation to the mean value, of the force components (including cutting resistance force, driving force, and joint reaction force) for two chip thickness cases, $d_1$ and $d_2$. The results show that, at each cutting depth, the CV values are relatively uniform: the CV values for $d_1$ and $d_2$ vary around approximately 31.3 % and 20.7 %, respectively. Additionally, increasing the chip thickness results in a reduced variation of the force components during operation, herein $\mathrm{CV}(d_1)/\mathrm{CV}(d_2)$ is approximately the ratio $d_2/d_1$. This can be explained by the fact that, with a larger chip thickness, a greater number of teeth $n_c$ are engaged in cutting at a given time, thereby decreasing the fluctuation range of the force components.

To compare the variation of force-related factors with increasing the cutting depth, Fig. 16 illustrates a comparison between the mean values of the force components as the thickness increases from $d_1$ to $d_2$. In this figure, the markers represent the values calculated from Fig. 12 (cutting resistance forces), Fig. 13 (driving forces), and Fig. 14 (joint reaction forces), while the solid line denotes the fitted relation $y = 4.08x$ with a correlation coefficient $R^2 = 0.98$.

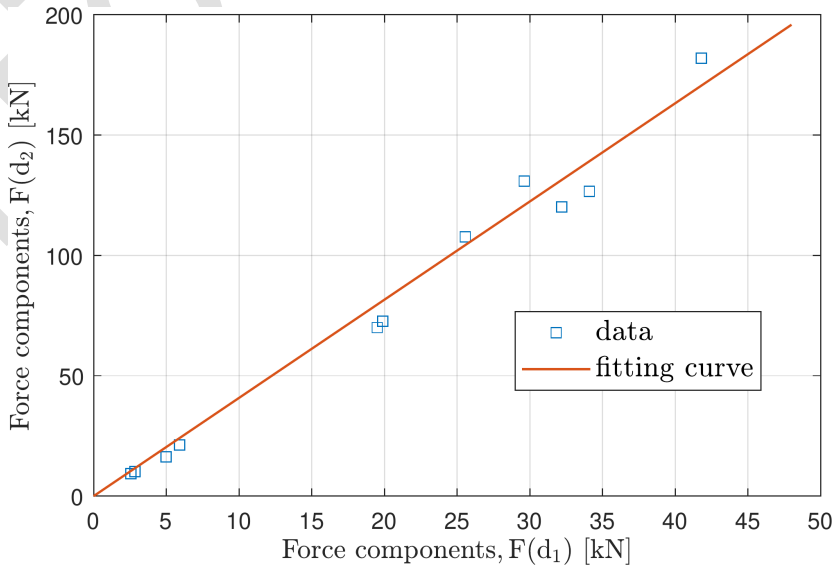


Fig. 16. Variation of the mean values of the force components with changing the cutting depth

These results indicate that the coefficient $4.08$ (i.e., variation level of the force components) is significantly larger than the ratio $2.25(= 1.5^2)$. This suggests that, in addition to the effect of the instantaneous cutting thickness $h(t)$, as discussed above, the increase in cutting thickness is also accompanied by an increase in the number of teeth $n_c$ simultaneously engaged in cutting.

## 6. Conclusions

Through the kinematic and dynamic analysis of the excavator equipped with an integrated drum cutter for dredging tasks, the present work studies the operating characteristics of the new equipment compared to the original bucket. This analysis is essential for designing and integrating new equipment into existing excavators and for selecting appropriate machines to meet specific construction needs, particularly in complex dredging operations. Based on a case study of the PC800 machine, the following specific conclusions can be drawn:

The integrated drum cutter significantly extends both the excavation depth (deeper than 15 m) and working area (approximately doubled) beyond the capabilities of the original bucket. This enhancement highlights a substantial improvement in operational reach and performance, providing a strong basis for further structural modifications aimed at optimizing the excavator's efficiency in channel excavation and other specialized tasks. The kinematic analysis establishes the explicit relationship between the motions of the individual driving cylinders and the cutting speed of the drum cutter, thereby clarifying the contribution of each cylinder to the overall motion of the drum cutter. The use of a long boom results in the cutting drum speed being more than 30 times higher than the speed of the driving cylinder.

Based on the established model, the dynamic characteristics of the equipment that differ from those of a conventional excavator have been identified. The cutting layer thickness has a significant influence on the variations of cutting force components, driving forces, and joint reaction forces. An increase in cutting depth leads to reduced relative fluctuations of these forces, while their absolute magnitudes increase substantially due to the increase in the cutting layer thickness and the number of teeth engaged simultaneously.

The insights derived from the kinematic and dynamic analysis provide essential data for optimizing cylinder movement/driving to meet the operational demands and conditions of the drum cutter. Future research directions may include investigating the operational performance of the equipment when it is installed on a floating pontoon, in which wave conditions and the parameters of the pontoon must be taken into account.

## References

[1] Bray, N., Cohen, M., Dredging for development, International Association of Dredging Companies, 2004.

[2] Cao, L., Wang, L., Cao, L., Gu, Y., Dynamics simulation of hydraulic excavator working device based on ADAMS, In: Advances in Mechanical Design: Proceedings of the 2017 International Conference on Mechanical Design (ICMD 2017), Springer, 2018, pp. 899–909. https://doi.org/10.1007/978-981-10-6553-8_60

[3] Ceresoli, F., Excavator with two or three arms: Dynamical behavior and structural implications, FME Transactions 48 (2) (2020) 272–280. https://doi.org/10.5937/fme2002272c

[4] Chen, Y., Chen, X., Yang, Q., Ouyang, Y., Dynamic stability analysis of backhoe dredger based on time domain method, Journal of Shanghai Jiaotong University (Science) 27 (3) (2022) 339–345. https://doi.org/10.1007/s12204-021-2272-x

[5] Chen, J., Zou, Z., Pang, X., Digging performance characterization for hydraulic excavator considering uncertainty during digging operation, Proceedings of the Institution of Mechanical Engineers – Part C: Journal of Mechanical Engineering Science 232 (5) (2018) 857–871. https://doi.org/10.1177/0954406217692843

[6] Denavit, J., Hartenberg, R. S., A kinematic notation for lower-pair mechanisms based on matrices, Journal of Applied Mechanics 22 (2) (1955) 215–221. https://doi.org/10.1115/1.4011045

[7] Deshmukh, S., Raina, A. K., Murthy, V. M. S. R., Trivedi, R., Vajre, R., Roadheader – A comprehensive review, Tunnelling and Underground Space Technology 95 (2020) No. 103148. https://doi.org/10.1016/j.tust.2019.103148

[8] Du, C.-L., Liu, S.-Y., Cui, X.-X., Li, T.-J., Study on pick arrangement of shearer drum based on load fluctuation, Journal of China University of Mining and Technology 18 (2) (2008) 305–310. https://doi.org/10.1016/S1006-1266(08)60065-6

[9] Edwards, D. J., Holt, G. D., Health and safety issues relating to construction excavators and their attachments, Engineering, Construction and Architectural Management 15 (4) (2008) 321–335. https://doi.org/10.1108/09699980810886838

[10] Goktan, R. M., Gunes, N., A semi-empirical approach to cutting force prediction for point-attack picks, Journal of the Southern African Institute of Mining and Metallurgy 105 (2005) 257–264.

[11] Guan, D., Yang, N., Lai, J., Siu, M. F. F., Jing, X., Lau, C.-K., Kinematic modeling and constraint analysis for robotic excavator operations in piling construction, Automation in Construction 126 (2021) No. 103666. https://doi.org/10.1016/j.autcon.2021.103666

[12] Gui, K. D., Du, C. L., Jiang, H. X., Drum cutting specific energy consumption model built by cutting curves analysis, TELKOMNIKA Indonesian Journal of Electrical Engineering 11 (7) (2013) 4 122–4 128. https://doi.org/10.11591/telkomnika.v11i7.2869

[13] Guo, X., Mao, Y., Kang, K., Dynamic simulation research on hydraulic system of backhoe dredger excavator, In: Lecture Notes in Computer Science: Proceedings of the conference Human Centered Computing (HCC 2014), Springer, 2015, pp. 757–764. https://doi.org/10.1007/978-3-319-15554-8_66

[14] Hofstra, C. F., van Hemmen A. J. M., Miedema S. A., van Hulsteyn J., Describing the position of backhoe dredge buckets, Proceedings of Texas A&M 32nd Annual Dredging Seminar, Warwick, Rhode Island, June, Citeseer, 2000.

[15] Hongxin, C., Ke, F., Huanliang, L., Jinhua, H., Virtual prototype and experimental research on spatial kinematics of telescopic robotic excavator, International Journal of Advanced Robotic Systems 14 (3) (2017) No. 1729881417705305. https://doi.org/10.1177/1729881417705305

[16] Jang, J.-S., Yoo, W.-S., Kang, H., Cho, J.-W., Jeong, M.-S., Lee, S.-K., Cho, Y.-J., Lee, J.-W., Rostami, J., Cutting head attachment design for improving the performance by using multibody dynamic analysis, International Journal of Precision Engineering and Manufacturing 17 (3) (2016) 371–377. https://doi.org/10.1007/s12541-016-0046-4

[17] Jůza, M., Heřmánek, P., Influence of the excavator hydraulic system efficiency on the productivity, Research in Agricultural Engineering 69 (1) (2023) 18–27. https://doi.org/10.17221/77/2021-RAE

[18] Kondaszewski, M., Chomka, G., Construction project of a long reach compact excavator, Journal of Mechanical and Energy Engineering 4 (4) (2020) 341–356. https://doi.org/10.30464/jmee.2020.4.4.341

[19] Krikun, V. Y., Manasyan, V. G., Calculation of the main parameters of hydraulic excavators with working equipment backhoe, Publishing House: ASV, 2001. (in Russian)

[20] Kumara, J. M., LakmalPerera, H. S., Design of a barge for small scale excavator in narrow canal, International Research Journal of Mathematics, Engineering & IT 4 (10) (2017) 1–18.

[21] Lee J., Kim B., Sun D., Han C., Ahn Y., Development of unmanned excavator vehicle system for performing dangerous construction work, Sensors 19 (22) (2019) No. 4853. https://doi.org/10.3390/s19224853

[22] Lever P. J. A., Wang F.-Y., Intelligent excavator control system for lunar mining system, Journal of Aerospace Engineering 8 (1) (1995) 16–24. https://doi.org/10.1061/(ASCE)0893-1321(1995)8:1(16)

[23] Liu, J., Ma, C., Zeng, Q., Gao, K., Discrete element simulation of conical pick's coal cutting process under different cutting parameters, Shock and Vibration 2018 (2018) No. 7975141. https://doi.org/10.1155/2018/7975141

[24] Mäkinen, P., Toward vision-based control of heavy-duty and long-reach robotic manipulators, Ph.D. thesis, Tampere University, Tampere, 2023.

[25] McConville, J. B., Introduction to mechanical system simulation using Adams, Ann Arbor, SDC publications, 2015.

[26] McLellan, T. N., Hopman, R. J., Innovations in dredging technology: Equipment, operations, and management, Report ERDC TR-DOER-5, U.S. Army Engineer Research and Development Center, 2000.

[27] Miedema, S. A., Dredging engineering: Special topics, TU Delft OPEN Books, 2019. https://doi.org/10.5074/t.2019.004

[28] Patel, B. P., Prajapati, J. M., A review on kinematics of hydraulic excavator's backhoe attachment, International Journal of Engineering Science and Technology 3 (3) (2011) 1 990–1 997.

[29] Reine, K., Clarke, D., Dickerson, C., Characterization of underwater sounds produced by a backhoe dredge excavating rock and gravel, Report ERDC TN-DOER-E36, U.S. Army Engineer Research and Development Center, 2012.

[30] Ryan, R. R., ADAMS—Multibody system analysis software, In: Multibody systems handbook, Schiehlen, W. (eds), Springer, 1990, pp. 361–402. https://doi.org/10.1007/978-3-642-50995-7_21

[31] Shestakov, V., Bezkorovainyy, P., Franz, T., Determination of the working area of a hydraulic excavator, E3S Web of Conferences 177 (2020) No. 03017. https://doi.org/10.1051/e3sconf/202017703017

[32] Williams, B., Commercial developments and their impact on maritime heritage: The Northern Ireland experience, International Journal of Nautical Archaeology 30 (1) (2001) 5–11. https://doi.org/10.1111/j.1095-9270.2001.tb01352.x

[33] Xie, C., Chen, M., Wang, L., Agee, C., Yao, S., Zheng, J., Liu, J., Xie, J., Ou, W., Xiao, J., Chen, W., A study on the performance modeling method for a deep-sea cobalt-rich crust mining vehicle, Minerals 12 (12) (2022) No. 1521. https://doi.org/10.3390/min12121521

[34] Yu, H. Y., Yuan, M. H., Deng, K., Dong, R., Kinematic and dynamic simulation analysis of hydraulic excavator's working equipment based on ADAMS, MATEC Web of Conferences 63 (2016) No. 02020. https://doi.org/10.1051/matecconf/20166302020

[35] Yu, X., Wang, Z., Li, Z., Sun, C., Design and kinematics analysis of four-linkage excavator, Proceedings of the 2019 International Conference on Robotics, Intelligent Control and Artificial Intelligence, 2019, pp. 605–610. https://doi.org/10.1145/3366194.3366302

[36] Zhang, L., Zhao J., Long P., Wang L., Qian L., Lu F., Song X., Manocha D., An autonomous excavator system for material loading tasks, Science Robotics 6 (55) (2021) No. eabc3164. https://doi.org/10.1126/scirobotics.abc3164

[37] Zhang, Q., Han, Z., Zhang, M., Zhang, J., New model for predicting instantaneous cutting rate of axial-type roadheaders, KSCE Journal of Civil Engineering 21 (2017) 168–177. https://doi.org/10.1007/s12205-016-0433-5

[38] Zou, Z., Chen, J., Pang, X., Optimum dimensional synthesis for the working mechanism of a hydraulic excavator to improve the digging performance, Proceedings of the Institution of Mechanical Engineers – Part K: Journal of Multi-body Dynamics 232 (3) (2018) 357–370. https://doi.org/10.1177/1464419317736675

[39] Zou, Z., Pang, X., Chen, J., Comprehensive theoretical digging performance analysis for hydraulic excavator using convex polytope method, Multibody System Dynamics 47 (2019) 137–164. https://doi.org/10.1007/s11044-019-09686-0